Matematisk-fysiske Meddelelser
udgivet af
Det Kongelige Danske Videnskabernes Selskab
Bind **35,** nr. 9

Mat. Fys. Medd. Dan. Vid. Selsk. **35,** no. 9 (1966)

RANGE-ENERGY RELATIONS FOR LOW-ENERGY IONS

BY

HANS E. SCHIØTT

København 1966
Kommissionær: Munksgaard

CONTENTS

Synopsis

Projected ranges are calculated for low-energy light particles in heavy substances (e.g. 20 keV deuterons in gold), together with straggling in projected range, assuming randomness of stopping material. The projected range turns out to be considerably less than the range along the path, and the distribution in projected range is very broad. The range ratio $\bar{R}_p/\bar{R}$ as well as the relative straggling $\Delta\overline{R_p^2}/\bar{R}_p^2$, are independent of stopping substance when a reduced energy measure, ε, is used, and are not strongly dependent on the atomic number of the projectile.

As an extension of earlier work are presented range-energy tables covering a large number of combinations of incoming particle and stopping substance.

PRINTED IN DENMARK
BIANCO LUNOS BOGTRYKKERI A/S

§ 1. Introduction

The purpose of the present paper is to study in detail some aspects of range distributions and thus to supplement the results in a previous paper, "Range Concepts and Heavy Ion Ranges" (LINDHARD, SCHARFF and SCHIØTT (1963) – in the following referred to as LSS). Of the problems treated in the following, one arose from a discussion of the recent measurements by CHU and FRIEDMAN (1965), where projected ranges were observed for 20 keV deuterons in aluminium and gold. The projected ranges found by CHU and FRIEDMAN were considerably smaller than the theoretical range along the path, which was somewhat unexpected since the ranges of light particles as protons, deuterons, etc. are normally little influenced by scattering effects. In § 2, consequently, the projected range is calculated as function of energy in the case of $Z_1 \ll Z_2$, where Z_1 and Z_2 are atomic numbers of incoming particle and stopping material, respectively. It is shown that, at low energies, the projected range may become an order of magnitude less than the range along the path. Calculations giving the fluctuation in projected range are also included.

In § 3 are presented numerical calculations on range along path as function of energy, performed since the appearance of LSS.

Integral equations describing the distribution in projected range are discussed in the Appendix. It should be emphasized that calculations in LSS, as well as in the present paper, are based on the assumption of randomness in the stopping substance. Caution should therefore be observed in comparisons between these theoretical results and experimentally determined ranges in crystals, where special directional effects may come into play, cf. e.g. KORNELSEN et al. (1964), and LINDHARD (1965).

General aspects of projected range calculations

An energetic charged particle loses energy by electronic and nuclear collisions, but is deflected by nuclear collisions only (BOHR, 1948). At high particle velocities the electronic stopping is completely dominating, the

nuclear stopping being $\sim 10^3$ times smaller than electronic stopping. This picture is valid for e.g. α-particles from radioactive decay, and in general for $v > v_1 = v_0 Z_1^{2/3}$, where $v_0 = e^2/\hbar$. At lower velocities, i.e. $v < v_1$, the electronic stopping is nearly proportional to velocity (LINDHARD and SCHARFF, 1961) and may still remain dominating for $Z_1 < Z_2$. For heavy particles, and with decreasing velocity, nuclear stopping gradually takes over relative to electronic stopping to form the major part of the energy loss.

Accordingly, it is natural, when calculating projected ranges, to divide in two groups. In the first group the total range is determined by electronic stopping solely, the nuclear collisions being responsible for scattering only. This is the simplest case, the solution of which is well-known for light particles at high energies, e.g. MeV-protons, α-particles, etc. It is also the case to be discussed in the following, but for particles at low energies.

In the second group the energy loss in nuclear collisions is an essential part of the total energy loss, so that the total range is partially determined by nuclear stopping. This case, which is the more complicated except when electronic stopping is much less than nuclear stopping, was treated in LSS.

Brief review of the main features of LSS

In LSS a comprehensive theoretical treatment of range-energy relations for slow heavy ions was attempted. The treatment was based on a universal nuclear stopping cross section, S_n, calculated from a Thomas-Fermi model of the interaction between heavy ions, and an electronic stopping cross section, S_e, proportional to v, the velocity of the incoming particle.

When energy and range are measured in the dimensionless parameters ε and ϱ, where

$$\varepsilon = E \cdot \frac{aM_2}{Z_1 Z_2 e^2 (M_1 + M_2)} \quad , \tag{1}$$

$$\varrho = RNM_2 \cdot 4\pi a^2 \frac{M_1}{(M_1 + M_2)^2} \quad , \tag{2}$$

(a being the screening parameter in the Thomas-Fermi potential $a = a_0 \cdot 0.8853\,(Z_1^{2/3} + Z_2^{2/3})^{-1/2}$) the nuclear stopping power, i.e. $(d\varepsilon/d\varrho)_n$ is a function of ε only, independent of incoming particle and stopping substance (Fig. 1). In the same units the electronic stopping power is represented by $(d\varepsilon/d\varrho)_e = k\varepsilon^{1/2}$, where

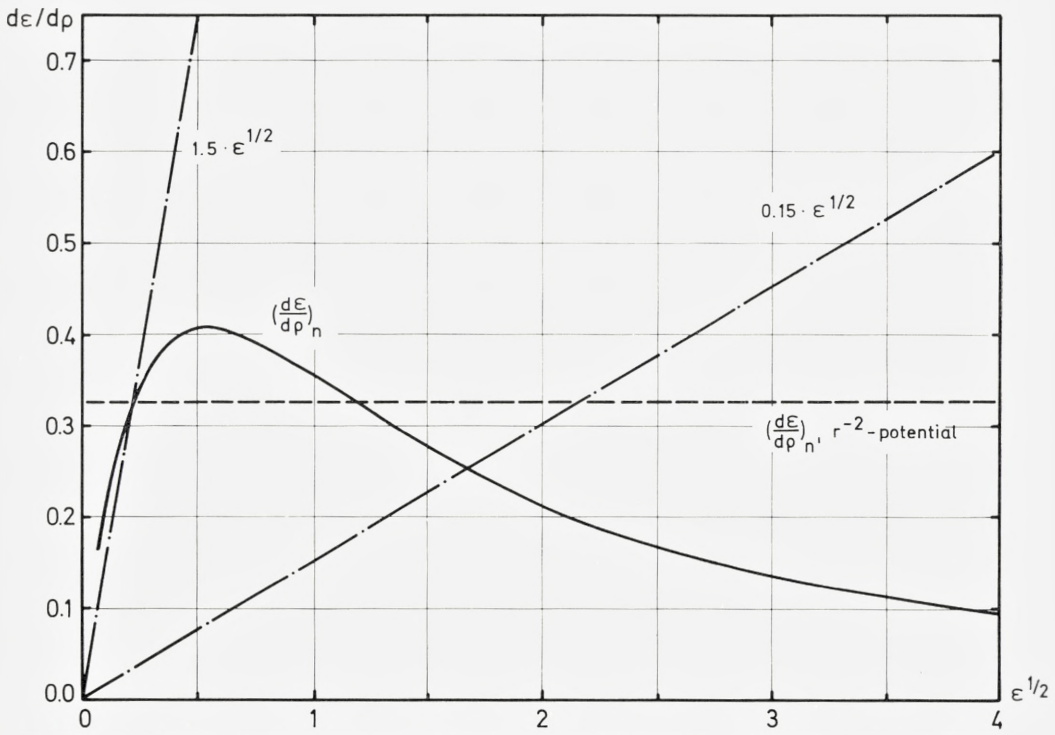

Figure 1. Nuclear and electronic stopping powers in reduced units. Full-drawn curve represents the Thomas-Fermi nuclear stopping power, the dot-and-dash lines the electronic stopping, (3), for $k = 0.15$ and $k = 1.5$.

$$k = \xi_e \cdot \frac{0.0793 \cdot Z_1^{1/2} Z_2^{1/2} (A_1 + A_2)^{3/2}}{(Z_1^{2/3} + Z_2^{2/3})^{3/4} \cdot A_1^{3/2} \cdot A_2^{1/2}}, \quad \xi_e \approx Z_1^{1/6}. \tag{3}$$

k is of order of $0.1 - 0.2$ for $Z_1 \gtrsim Z_2$, and only when $Z_1 \ll Z_2$, can k become larger than unity. The estimate, (3), of k, which is based on Thomas-Fermi arguments, gives a good over-all fit to experiments. Oscillations around the theoretical k-value, due to atomic shell effects, have been observed, especially for low atomic numbers (Ormrod and Duckworth, 1963; Fastrup, Hvelplund and Sautter, 1966). Two representative cases of electronic stopping, i.e. $k = 0.15$ and $k = 1.5$, are included in Fig. 1. The nuclear stopping power calculated from an inverse second power potential between the atoms is also included. This stopping power turns out to be constant, leading to a linear range energy relation (Bohr, 1948; Nielsen, 1956).

By numerical integration of the inverse total stopping power, $((d\varepsilon/d\varrho)_n + (d\varepsilon/d\varrho)_e)^{-1}$, for different values of the electronic stopping parameter, k, curves $\bar{\varrho} = \varrho_k(\varepsilon)$ were obtained and plotted in LSS. The range $\bar{\varrho}$ is the total length of the particle path. The penetration depth (projected range) is less than this quantity – the more so the larger the mass ratio $\mu = M_2/M_1$. The ratio $\bar{\varrho}_p/\bar{\varrho}$ was calculated by a series development to first order in μ for $\mu \ll 1$ and in a few cases for $\mu = 1$ and $\mu = 2$.

§ 2. Light Particles in Heavy Substances

Mean projected range

The equation governing the average projected range may be written down directly (cf. LSS) or may e.g. be derived from the equations describing the distribution in penetration depth, cf. Appendix. The equation is

$$1 = N \int d\sigma_{n,e}(\bar{R}_p(E) - \bar{R}_p(E - T) \cdot \cos \varphi), \tag{4}$$

where N is the number of target atoms per cm^3, $d\sigma_{n,e}$ is the differential cross section for a collision specified by energy loss T_n to the nucleus and $\sum_i T_{ei}$ to electrons, $T = T_n + \sum_i T_{ei}$, and φ is the deflection angle in the laboratory system.

Solution of equation (4) now proceeds as in LSS. The first approximation to be introduced is a series development to first order of the term $\bar{R}_p(E - T)$. Since

$$T_n < \frac{4M_1M_2}{(M_1 + M_2)^2} \cdot E = \gamma E,$$

and $\gamma \ll 1$ in the case of $4M_1 \ll M_2$, this is permissible. Moreover, the differential cross section favours strongly small energy transfers, $T_n \ll \gamma E$, and, further, energy loss to electrons in a single collision is always small compared to particle energy. Equation (4) then reads

$$1 = \bar{R}_p(E) \cdot N \int d\sigma_{n,e}(1 - \cos\varphi) + \frac{d\bar{R}_p(E)}{dE} \cdot N \int d\sigma_{n,e} \cdot T \cos\varphi. \tag{5}$$

By introducing the quantities

$$\left.\begin{aligned} \lambda_{tr}^{-1} &= N \int d\sigma_{n,e}(1 - \cos\varphi), \\ S_{tr} &= \int d\sigma_{n,e} T \cos\varphi, \end{aligned}\right\} \tag{6}$$

the solution of equation (5) may be written as

$$\bar{R}_p(E) = \int_0^E \frac{dE'}{NS_{tr}(E')} \exp\left[\int_E^{E'} \frac{dE''}{\lambda_{tr}(E'') \cdot NS_{tr}(E'')}\right]. \tag{7}$$

Equ. (7) should be a good approximation to the average projected range when γ is small.

In case of $\mu = M_2/M_1 \ll 1$ (in which case also $\gamma \ll 1$) the scattering angle φ is always very small, and $\bar{R}_p$ is not much different from $\bar{R}$. When, on the contrary, $\mu \gg 1$, there is a possibility of large scattering angles, and one cannot beforehand exclude the possibility that the projected range becomes considerably smaller than the path length.

In order to estimate λ_{tr} and S_{tr} in (6), we separate electronic and nuclear collisions, i.e. we put $d\sigma_{n,e} = d\sigma_n + d\sigma_e$, noting that $\varphi = 0$ in electronic collisions, while in nuclear collisions φ is given by

$$\cos\varphi = \left(1 - \frac{1+\mu}{2}\frac{T_n}{E}\right)\left(1 - \frac{T_n}{E}\right)^{-1/2} \cong 1 - \frac{\mu}{2}\frac{T_n}{E}, \quad \text{when } \gamma \ll 1. \tag{8}$$

We thereby obtain

$$\left.\begin{aligned} S_{tr}(E) &\cong S_e(E) + S_n(E) - \frac{\mu}{2} \cdot \frac{\Omega^2(E)}{E}, \quad \Omega^2(E) = \int T_n^2 d\sigma_n, \\ \lambda_{tr}^{-1}(E) &\cong N \cdot \frac{\mu}{2} \cdot \frac{S_n(E)}{E}. \end{aligned}\right\} \tag{9}$$

Since $k \gtrsim 1$, for $Z_1 \ll Z_2$, the electronic stopping is a major part of the energy loss even at very low energies (cf. Fig. 1). We then disregard nuclear stopping compared to electronic stopping and put $S_{tr} \cong S_e(E)$.

In actual calculations it is convenient to introduce the variables ϱ and ε given by (1) and (2). With this rescaling of units equation (7) may be written

$$\frac{\bar{\varrho}_p(\varepsilon)}{\varrho_e(\varepsilon)} = \frac{1}{\varrho_e(\varepsilon)} \int_0^{\varepsilon} \frac{d\varepsilon'}{(d\varepsilon'/d\varrho)_e} \exp\left[\int_{\varepsilon}^{\varepsilon'} \frac{d\varepsilon''(\mu/2)(d\varepsilon''/d\varrho)_n}{(d\varepsilon''/d\varrho)_e \cdot \varepsilon''} \right]. \tag{10}$$

Since we have neglected nuclear stopping compared to electronic stopping, $\bar{\varrho}_p(\varepsilon)$, given by (10), should be compared with the extrapolated electronic range, $\varrho_e(\varepsilon) = 2k^{-1}\varepsilon^{1/2}$ (cf. § 3), and although the absolute value of $\bar{\varrho}_p(\varepsilon)$ might be somewhat in error, the ratio $\bar{\varrho}_p(\varepsilon)/\varrho_e(\varepsilon)$ is expected to be rather accurate. Moreover, it may be shown that, if the nuclear stopping contributions to S_{tr} are not neglected compared to electronic stopping, the ratio between projected range and range along path is very nearly equal to $\bar{\varrho}_p(\varepsilon)/\varrho_e(\varepsilon)$, as given by equ. (10). Accordingly, we drop the subscript $_e$ in $\varrho_e(\varepsilon)$, simply writing $\bar{\varrho}_p(\varepsilon)/\bar{\varrho}(\varepsilon)$.

Inserting $(d\varepsilon/d\varrho)_e = k\varepsilon^{1/2}$ in (10), we notice that $\bar{\varrho}_p(\varepsilon)/\bar{\varrho}(\varepsilon)$ depends on the parameters μ and k through the ratio μ/k only; moreover, this ratio is very nearly independent of the target material for a specified projectile. We may then, by a single integration, calculate e.g. the projected range of protons in all heavy materials. Equ. (10) may be solved analytically if $(d\varepsilon/d\varrho)_n$ is equal to a constant, λ, corresponding to the r^{-2}-potential between atoms. One then finds

$$\frac{\bar{\varrho}_p(\varepsilon)}{\bar{\varrho}(\varepsilon)} = 1 - xe^x Ei(x), \quad x = \frac{\mu\lambda}{k\varepsilon^{1/2}} = \mu \cdot \frac{S_n}{S_e}, \tag{11}$$

where $\lambda = 0.327$ (cf. Fig. 1), and the exponential integral $Ei(x)$ is defined by

$$Ei(x) = \int_x^{\infty} \frac{e^{-t}}{t}\, dt.$$

Formula (11) is expected to be fairly accurate for ε-values less than ~ 5 (cf. Fig. 1) and to overestimate the nuclear stopping at higher energies, thereby giving too small values of $\bar{\varrho}_p/\bar{\varrho}$. For large values of x, i.e. for low energies, we may use the approximate relation

$$\frac{\bar{\varrho}_p(\varepsilon)}{\bar{\varrho}(\varepsilon)} \cong \frac{1}{x}\left(1 - \frac{2}{x}\right). \tag{12}$$

In Fig. 2 are shown $\bar{\varrho}_p/\bar{\varrho}$ given by (11) together with a numerical integration of (10) using the Thomas-Fermi nuclear stopping power. Curves are pre-

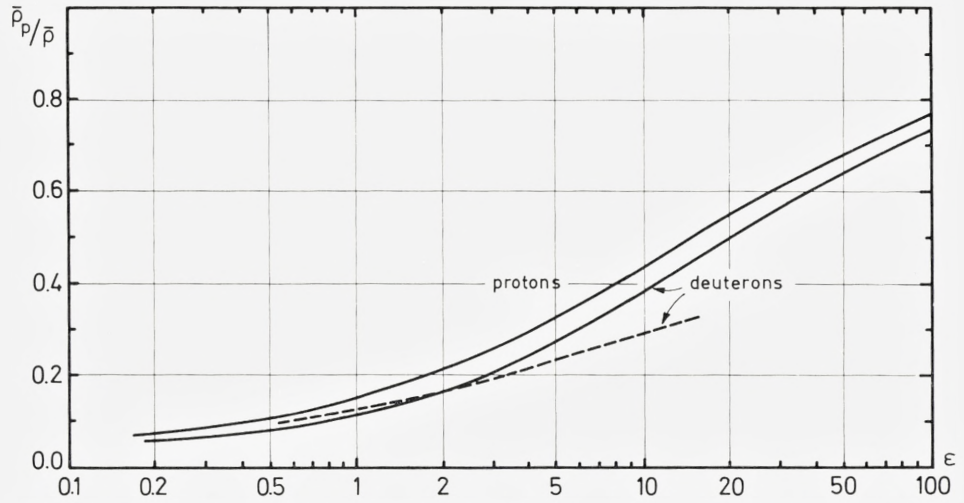

Figure 2. Projected range corrections for protons (μ/k = 13.1), and deuterons (μ/k = 18.3). Dashed curve represents the analytical solution (11) for deuterons, i.e. corresponding to constant nuclear stopping power.

sented for protons (μ/k = 13.1) and deuterons (μ/k = 18.3). It is remarkable that the dependence on μ/k is not very strong, and, moreover, that values of μ/k for other light particles fall in between those for protons and deuterons. Accordingly, an uncertainty in the theoretical estimate of k does not affect the value of $\bar{\varrho}_p/\bar{\varrho}$ in first approximation.

In case of mixed stopping substance, one may estimate the projected range by rather simple averages. If there are two elements, a and b, in the target, one finds $\bar{R}_p \approx \bar{R}_{p,a} \cdot \bar{R}_{p,b}/(x_a \cdot \bar{R}_{p,b} + (1 - x_a)\bar{R}_{p,a})$, where $\bar{R}_{p,a}$ and $\bar{R}_{p,b}$ are the projected ranges in a and b, and x_a and $1 - x_a$ are the relative abundances of a and b. The formula is valid if $\bar{R}_p$ in the pure elements of the stopping substance is proportional to a common power of E, which is the case when A_1 is much less than the mass number of both a and b. In LSS a similar formula was quoted for the range along path in a mixed substance.

It should be mentioned that we have used a velocity proportional electronic stopping power. This approximation is valid for $v \lesssim v_1 = v_0 \cdot Z_1^{2/3}$ corresponding to $E \lesssim E_1 = A_1 \cdot Z_1^{4/3} \cdot 25$ keV. Note that the corresponding maximum permissible ε-value, ε_1, for a specified particle decreases with increasing Z_2. In cases of interest it turns out that $\varepsilon_1 \lesssim 50$. For $E > E_1$, the stopping power goes through a maximum and then decreases, joining smoothly the Bethe stopping power curve. In this region the nuclear

stopping is determined by Rutherford scattering, i.e. in ε-units $(d\varepsilon/d\varrho)_n = 1/2\,\varepsilon \cdot ln\ (1.29\varepsilon)$, $(\varepsilon > 10)$. Therefore, the ratio between electronic and nuclear stopping is nearly a constant, of order of 10^3. It turns out that we can put, with close approximation for $\varepsilon \lesssim 10 \cdot \varepsilon_1$,

$$\bar{\varrho}_p(\varepsilon) = \bar{\varrho}(\varepsilon) - \bar{\varrho}(\varepsilon_1) + \bar{\varrho}_p(\varepsilon_1). \tag{13}$$

Equ. (13) leads to the familiar conclusion that scattering is a low energy phenomenon, so that the path at high energies is a straight line in first approximation. We find immediately

$$\frac{\bar{\varrho}_p(\varepsilon)}{\bar{\varrho}(\varepsilon)} = 1 - \frac{\bar{\varrho}(\varepsilon_1) - \bar{\varrho}_p(\varepsilon_1)}{\bar{\varrho}(\varepsilon)}. \tag{14}$$

From this equation it is seen that $\bar{\varrho}_p(\varepsilon)/\bar{\varrho}(\varepsilon)$ increases more rapidly for the true electronic stopping than for the velocity proportional stopping, since the former case gives a larger range than does the latter.

Formula (13) may be used in an intermediate energy region, where the correction from true to projected range still is $\gtrsim 5\,\%$. In this region it gives directly the correction to a measured projected range, namely the constant term $\bar{\varrho}(\varepsilon_1) - \bar{\varrho}_p(\varepsilon_1)$, which in actual cases may be calculated by means of Table 2 and Fig. 2. For very high energies ($\gtrsim 1$ MeV for protons e.g.) the correction $\bar{\varrho}(\varepsilon_1) - \bar{\varrho}_p(\varepsilon_1)$ is negligible, and the difference $\bar{R} - \bar{R}_p$ is determined by the small multiple scattering at high energies.

Fluctuations in projected range

A projected range becomes smaller than the corresponding true range if the particle during slowing-down undergoes numerous collisions with appreciable deflections. Because of such deflections the width of the distribution in projected range may be considerable, and it is therefore of interest to calculate e.g. the fluctuation in projected range. Equations governing fluctuations are derived in the Appendix, and it turns out to be necessary to treat simultaneously the average square of the projected range, $\overline{R_p^2}$, and of the perpendicular range $\overline{R_\perp^2}$.

The equations are of the same type as equ. (4), and may be solved by the same approximations if one knows the average projected range, which enters as a source term. In Fig. 3 are shown the results of numerical calculations for protons and deuterons. The curve illustrating the relative straggling in projected range shows that at low energies, i.e. $\varepsilon \lesssim 1$, the distribution

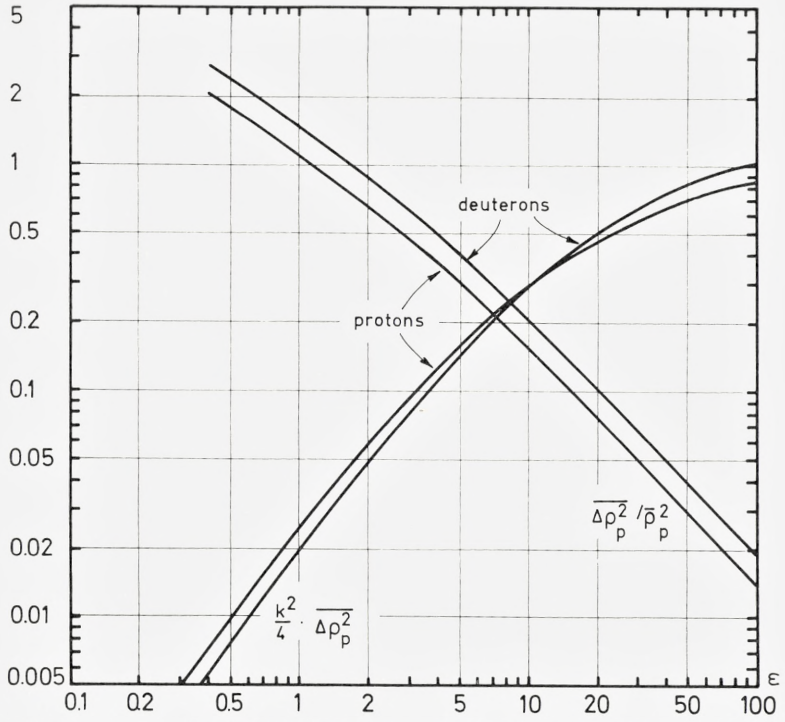

Figure 3. The square of absolute and relative straggling in projected range for protons and deuterons, calculated by means of the Thomas-Fermi nuclear stopping power (Fig. 1).

becomes very broad, actually the full width at half maximum is expected to be larger than the average value by a factor $\sim 2-3$. It is therefore expected that a fraction of the incoming particles is ejected from the target.

Comparison with experiments

The distribution in projected range of N^{15} ions ($\mu/k \approx 13.5$) with energies 0.5 – 6 MeV has been measured in Au by PHILLIPS and READ (1963). The depth distribution was found by observing the yield of a resonance in the N^{15} $(p, \alpha\gamma)$ C^{12} reaction. The present theory should apply with some reservation ($k = 0.95$, so that nuclear stopping is not quite negligible), and the average projected ranges agree with theory within $\sim 10\,\%$. The theoretical straggling, $(\overline{\Delta\varrho_p^2})^{1/2}$, is larger than the experimental value found by measuring the width of the Gaussian part of the distribution by $\sim 20-50\,\%$. This result is not very surprising, since the distribution is not a Gaussian, and

a skewness in the distribution may contribute essentially to the straggling. CHU and FRIEDMAN (1965) measured, by use of the D – D fusion process, the penetration in Al and Au of 20 keV deuterons in different molecular ions (D^+, D_2^+, HD^+, etc.) and found the distribution to depend on the molecular state of the incoming deuterons. Such effects are not fully understood. Qualitatively, the average projected range and the straggling agree with theory. In both cases the velocity proportional stopping may be applied.

§ 3. Length of Particle Path

Since the appearance of LSS a large number of different range measurements have been performed, and some of the curves presented in LSS have been used in the analysis of experimental results. In order to compare more precisely theory and experiments, I have calculated several range-energy curves for k-values other than those presented in LSS.

At low energies, ($\varepsilon \lesssim 1$), and not too large values of the electronic stopping parameter, k, $k \lesssim 0.5$, the nuclear stopping is dominating. Therefore, the curves $\bar{\varrho} = \varrho_k(\varepsilon)$ for different k-values $0.1 \lesssim k \lesssim 0.5$ are closely spaced and interpolations for intermediate k-values are easily performed. At higher energies, where the electronic stopping becomes the more significant energy loss mechanism, another plot is more appropriate, cf. LSS. If nuclear stopping is disregarded, the range is given by the extrapolated electronic range

$$\varrho_e(\varepsilon) = \int_0^{\varepsilon} \left(\frac{d\varepsilon'}{d\varrho}\right)_e^{-1} d\varepsilon'. \tag{15}$$

As shown in LSS, ϱ_e is given by

$$\varrho_e(\varepsilon) = \varrho_k(\varepsilon) + A(k,\varepsilon), \tag{16}$$

where the nuclear range correction A may be calculated simply by means of the stopping powers. A is nearly constant at high energies. In case of velocity proportional electronic stopping, the extrapolated electronic range is given by $\varrho_e(\varepsilon) = 2/k \cdot \varepsilon^{1/2}$.

Values of $\varrho_k(\varepsilon)$ for $0.002 \leq \varepsilon \leq 600$ for several k-values in the interval $0.05 < k < 1.6$ are presented in Table 1. The function $(d\varepsilon/d\varrho)_n$ is also included. In Table 2 are given values of the function $(k/2) \cdot A(k,\varepsilon)$ for $1 \leq \varepsilon \leq 600$ for the same k-values. The asymptotic values of A at high

energies are shown in Fig. 4. Some of the results in Tables 1 and 2 were utilized in plotting the curves presented in LSS.

The range straggling, $\overline{\Delta\varrho_k^2}(\varepsilon)$, was also calculated in LSS for a few values of k. At low energies, where $S_e \ll S_n$, a small error in k is not significant, but at high energies it is of interest to eliminate, as far as possible,

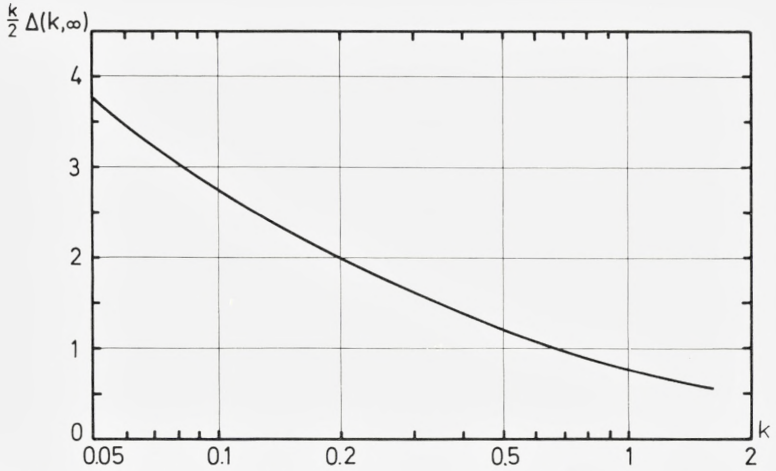

Figure 4. Asymptotic value of nuclear range correction $\Delta(k,\varepsilon)$ for large ε, cf. (16).

uncertainties in the theoretical estimate of k. It turns out that in the case of straggling the quantity $\overline{\Delta\varrho_k^2}/\varrho_k^3$ is a slowly varying function of k. Accordingly, a value of this quantity, obtained from LSS, may be compared with an experimentally determined average range to give a more precise estimate of $\overline{\Delta R^2}$.

Acknowledgments

I am much indebted to Professor J. Lindhard for his interest in the present work and his always kind advice and valuable criticism.

I want to express my thanks to P. V. Thomsen for help and criticism, and to Susann Toldi for assistance in the preparation of the manuscript.

Institute of Physics
University of Aarhus

TABLE 1.

Range along path, $\varrho_k(\varepsilon)$, for different values of electronic stopping parameter, k.

ε \ k	0.05	0.08	0.09	0.1	0.11	0.12	0.13	0.14	0.15	0.16	0.18
0.002	0.0260	0.0257	0.0256	0.0254	0.0254	0.0253	0.0252	0.0251	0.0250	0.0249	0.0248
0.004	0.0404	0.0399	0.0398	0.0395	0.0394	0.0393	0.0391	0.0390	0.0389	0.0387	0.0385
0.006	0.0522	0.0516	0.0514	0.0511	0.0509	0.0508	0.0505	0.0504	0.0503	0.0500	0.0497
0.008	0.0627	0.0619	0.0617	0.0610	0.0611	0.0609	0.0606	0.0605	0.0604	0.0600	0.0598
0.01	0.0722	0.0714	0.0711	0.0708	0.0704	0.0702	0.0699	0.0697	0.0696	0.0691	0.0689
0.02	0.114	0.112	0.111	0.111	0.110	0.110	0.109	0.109	0.109	0.108	0.107
0.04	0.181	0.178	0.177	0.176	0.175	0.175	0.174	0.173	0.172	0.171	0.170
0.06	0.241	0.236	0.235	0.234	0.232	0.231	0.230	0.229	0.228	0.227	0.225
0.08	0.296	0.290	0.288	0.287	0.285	0.284	0.282	0.281	0.279	0.278	0.275
0.1	0.348	0.341	0.339	0.337	0.335	0.333	0.331	0.330	0.328	0.326	0.323
0.2	0.592	0.578	0.574	0.570	0.566	0.562	0.558	0.555	0.551	0.547	0.540
0.4	1.06	1.02	1.01	1.00	0.995	0.986	0.977	0.969	0.960	0.952	0.936
0.6	1.52	1.46	1.45	1.43	1.42	1.41	1.39	1.37	1.36	1.34	1.32
0.8	1.99	1.91	1.88	1.86	1.84	1.82	1.79	1.77	1.75	1.73	1.69
1.0	2.47	2.36	2.33	2.29	2.26	2.24	2.20	2.17	2.14	2.12	2.07
2.0	5.09	4.75	4.65	4.56	4.46	4.38	4.29	4.20	4.13	4.05	3.91
4.0	11.1	9.94	9.61	9.38	9.02	8.77	8.52	8.28	8.07	7.87	7.49
6.0	17.7	15.4	14.7	14.3	13.6	13.1	12.7	12.3	11.9	11.5	10.9
8.0	24.5	20.8	19.7	19.1	18.0	17.3	16.7	16.0	15.5	15.0	14.0
10.0	31.5	26.1	24.6	23.6	22.3	21.4	20.5	19.6	18.9	18.2	17.0
20.0	65.6	50.6	47.0	44.3	41.4	39.2	37.1	35.3	33.7	32.2	29.6
40.0	126.0	90.9	83.4	77.4	71.8	67.2	63.2	59.7	56.6	53.7	48.9
60.0	176.0	124.0	113.0	104.0	96.3	89.8	84.1	79.2	74.8	70.8	64.2
100.0	261.0	178.0	161.0	148.0	136.0	126.0	118.0	111.0	105.0	98.4	88.7
200.0	421.0	280.0	252.0	229.0	210.0	195.0	181.0	169.0	159.0	150.0	134.0
400.0	653.0	425.0	381.0	346.0	316.0	292.0	271.0	252.0	237.0	223.0	199.0
600.0	832.0	537.0	481.0	436.0	397.0	366.0	339.0	316.0	297.0	279.0	249.0

TABLE 1 (continued).
Nuclear stopping power in reduced units, i. e. $(d\varepsilon/d\varrho)_n$ is included in the last column.

ε \ k	0.2	0.22	0.25	0.3	0.4	0.6	0.8	1.0	1.2	1.6	$(d\varepsilon/d\varrho)_n$
0.002	0.0246	0.0244	0.0242	0.0237	0.0230	0.0220	0.0210	0.0200	0.0192	0.0174	0.121
0.004	0.0419	0.0379	0.0375	0.0368	0.0357	0.0338	0.0321	0.0305	0.0291	0.0264	0.154
0.006	0.0494	0.0489	0.0484	0.0475	0.0460	0.0434	0.0411	0.0390	0.0371	0.0336	0.178
0.008	0.0593	0.0586	0.0580	0.0569	0.0551	0.0518	0.0490	0.0464	0.0441	0.0398	0.197
0.01	0.0682	0.0675	0.0668	0.0655	0.0633	0.0595	0.0562	0.0531	0.0504	0.0454	0.211
0.02	0.106	0.105	0.104	0.102	0.0983	0.0917	0.0860	0.0810	0.0765	0.0686	0.261
0.04	0.169	0.167	0.165	0.161	0.154	0.143	0.133	0.125	0.117	0.104	0.311
0.06	0.223	0.220	0.217	0.212	0.203	0.186	0.173	0.161	0.151	0.134	0.340
0.08	0.274	0.269	0.265	0.258	0.246	0.226	0.208	0.194	0.181	0.159	0.359
0.1	0.319	0.315	0.310	0.302	0.288	0.262	0.246	0.224	0.208	0.183	0.372
0.2	0.533	0.525	0.515	0.500	0.471	0.423	0.385	0.353	0.326	0.283	0.403
0.4	0.926	0.905	0.883	0.851	0.791	0.697	0.622	0.564	0.515	0.440	0.405
0.6	1.30	1.27	1.23	1.18	1.08	0.944	0.830	0.745	0.676	0.571	0.391
0.8	1.66	1.62	1.57	1.50	1.36	1.17	1.02	0.909	0.821	0.688	0.373
1.0	2.02	1.97	1.90	1.80	1.63	1.38	1.20	1.06	0.954	0.794	0.356
2.0	3.79	3.66	3.50	3.26	2.87	2.34	1.97	1.71	1.52	1.24	0.291
4.0	7.16	6.85	6.44	5.87	5.00	3.90	3.21	2.73	2.39	1.91	0.213
6.0	10.3	9.78	9.11	8.19	6.85	5.21	4.23	3.56	3.09	2.44	0.173
8.0	13.2	12.5	11.6	10.3	8.43	6.36	5.11	4.28	3.69	2.90	0.147
10.0	15.9	15.0	13.8	12.2	9.99	7.39	5.90	4.91	4.22	3.30	0.128
20.0	27.5	25.6	23.3	20.2	16.1	11.6	9.07	7.47	6.36	4.91	0.0813
40.0	44.9	41.6	37.4	32.1	25.1	17.6	13.6	11.1	9.42	7.21	0.0493
60.0	58.7	54.2	48.5	41.4	32.1	22.3	17.2	14.0	11.8	8.98	0.0362
100.0	80.8	74.3	66.3	56.2	43.3	29.8	22.8	18.5	15.5	11.8	0.0243
200.0	122.0	112.0	99.2	83.7	63.9	43.6	33.1	26.7	22.4	17.0	0.0139
400.0	180.0	165.0	146.0	123.0	93.1	63.1	47.8	38.4	32.2	24.3	0.0078
600.0	225.0	206.0	182.0	153.0	116.0	78.1	59.0	47.4	39.7	29.9	0.0056

TABLE 2.
Nuclear range correction, $k/2 \cdot \Delta(k, \varepsilon)$, cf. (16).

ε \ k	0.05	0.08	0.09	0.10	0.11	0.12	0.13	0.14	0.15	0.16	0.18
1	0.94	0.91	0.90	0.89	0.88	0.87	0.86	0.85	0.84	0.83	0.82
2	1.29	1.22	1.21	1.19	1.17	1.15	1.14	1.12	1.10	1.09	1.06
4	1.72	1.60	1.57	1.53	1.50	1.47	1.45	1.42	1.39	1.37	1.33
6	2.01	1.84	1.79	1.73	1.70	1.66	1.63	1.59	1.56	1.53	1.47
8	2.22	2.00	1.94	1.88	1.84	1.79	1.75	1.71	1.67	1.63	1.57
10	2.38	2.12	2.06	1.98	1.94	1.88	1.84	1.79	1.75	1.71	1.64
20	2.83	2.45	2.35	2.26	2.19	2.12	2.06	2.00	1.94	1.89	1.81
40	3.18	2.68	2.57	2.45	2.37	2.29	2.21	2.14	2.08	2.02	1.92
60	3.34	2.79	2.66	2.53	2.45	2.36	2.28	2.21	2.14	2.09	1.97
100	3.48	2.88	2.75	2.61	2.52	2.42	2.34	2.26	2.16	2.13	2.02
200	3.60	2.96	2.80	2.68	2.59	2.47	2.39	2.31	2.20	2.16	2.05
400	3.68	3.00	2.83	2.71	2.62	2.50	2.42	2.36	2.23	2.19	2.07
600	3.71	3.02	2.85	2.72	2.66	2.52	2.46	2.38	2.24	2.20	2.09

ε \ k	0.20	0.22	0.25	0.30	0.40	0.60	0.80	1.0	1.2	1.6
1	0.80	0.78	0.76	0.73	0.67	0.59	0.52	0.47	0.43	0.37
2	1.03	1.01	0.98	0.93	0.84	0.71	0.63	0.56	0.50	0.42
4	1.28	1.25	1.20	1.12	1.00	0.83	0.72	0.63	0.57	0.47
6	1.42	1.37	1.31	1.22	1.08	0.89	0.76	0.67	0.60	0.50
8	1.51	1.46	1.39	1.29	1.13	0.92	0.79	0.69	0.62	0.51
10	1.57	1.52	1.44	1.33	1.16	0.95	0.80	0.71	0.63	0.52
20	1.73	1.65	1.56	1.44	1.25	1.00	0.85	0.74	0.66	0.55
40	1.84	1.74	1.64	1.50	1.30	1.03	0.87	0.75	0.67	0.56
60	1.88	1.79	1.69	1.54	1.32	1.05	0.88	0.77	0.69	0.56
100	1.92	1.83	1.71	1.57	1.35	1.06	0.89	0.77	0.69	0.56
200	1.94	1.85	1.74	1.58	1.36	1.07	0.90	0.78	0.69	0.56
400	1.96	1.87	1.76	1.61	1.37	1.08	0.90	0.78	0.69	0.56
600	1.98	1.88	1.77	1.62	1.38	1.08	0.91	0.78	0.70	0.56

Appendix

Distribution in Projected Range

When a beam of particles is stopped in a substance, the individual paths of the particles are very different from each other. It is possible in principle to find the final distribution in space of the particles by means of electronic

computers, but with increasing energy of the particles and increasing number of atoms in the stopping material, such calculations become very intricate and expensive.

One may, however, derive analytical expressions governing the distribution in projected range, R_p, and in the perpendicular range, $R_\perp$. These expressions are integral equations, which are difficult to solve. Instead of attempting a direct solution, it is more fruitful to transform the distribution equation into equations describing the moments of the distribution. The latter may be solved by means of fair approximations, thereby supplying some information about the distribution functions too.

Consider a particle (Z_1, A_1) with energy E, moving in a substance (Z_2, A_2) in a direction specified by the angle ϑ with a certain direction in the substance (e.g. the surface normal), which is chosen as the z-axis. Define now a distribution function $p(E, z, \cos\vartheta)$ such that $p(E, z, \cos\vartheta)dz$ represents the probability that the final z-value comes between z and $z + dz$.

Define analogously a distribution function $q(E, r, \cos\vartheta)$ such that $q(E, r, \cos\vartheta) \cdot 2\pi r dr$ is the probability of finding the final distance from the z-axis between r and $r + dr$. The moments are given by

$$\langle z^m \rangle \equiv \langle R_p^m(E, \cos\vartheta) \rangle = \int_{-\infty}^{\infty} p(E, z, \cos\vartheta) \cdot z^m dz, \tag{A.1}$$

$$\langle r^m \rangle \equiv \langle R_\perp^m(E, \cos\vartheta) \rangle = \int_0^{\infty} q(E, r, \cos\vartheta) \cdot 2\pi r^{m+1} dr, \tag{A.2}$$

where we have introduced the expressions $R_p(E, \cos\vartheta)$ and $R_\perp(E, \cos\vartheta)$ for z and r, respectively. Clearly, $R_p(E, \cos\vartheta)$ is to be interpreted as the penetration depth of a particle originally moving in a direction specified by the angle ϑ, and $R_\perp(E, \cos\vartheta)$ is the final distance from the z-axis of the same particle.

Integral equations for $p(E, z, \cos\vartheta)$ and $q(E, r, \cos\vartheta)$ may be derived in analogy to the derivation of equation (3.1) in LSS, i.e. the equation governing the distribution in range along the path. We find readily

$$\left.\begin{aligned} &\cos\vartheta \cdot \frac{\partial p(E, z, \cos\vartheta)}{\partial z} = \\ &N \int d\sigma_{n,e} \int_0^{2\pi} \frac{d\alpha}{2\pi} \Big\{ p(E - T, z, \cos\vartheta\cos\varphi + \sin\vartheta\sin\varphi\cos\alpha) - p(E, z, \cos\vartheta) \Big\}, \end{aligned} \right\} \tag{A.3}$$

$$\left.\begin{aligned} &\sin\vartheta\cdot\frac{\partial q(E,r,\cos\vartheta)}{\partial r} = \\ &N\int d\sigma_{n,e}\int_0^{2\pi}\frac{d\alpha}{2\pi}\Big\{q(E-T,r,\cos\vartheta\cos\varphi+\sin\vartheta\sin\varphi\cos\alpha)-q(E,r,\cos\vartheta)\Big\}, \end{aligned}\right\} \quad (A.4)$$

where φ is the deflection of the incoming particle in the laboratory system, α being the azimuthal angle.

Equations (A. 3) and (A. 4) are valid under the same conditions as the corresponding equation (LSS (3.1)) describing the distribution in range along the path, i.e. the stopping substance should be a "random" system. The equation mentioned is contained in (A. 3), as may be seen by neglecting the angular dependence in (A. 3), putting $\vartheta = 0$. The same approximations as those introduced in the solution of the former equation may be employed in (A. 3) and (A. 4), i.e. we assume that the energy losses to electrons are small and separated from nuclear energy losses.

We shall not introduce the approximations at this stage, but at once turn to the moments of the distribution. Multiply (A. 3) by z^m and integrate over all z; analogously multiply (A. 4) by $2\pi r^{m+1}$ and integrate over all r, to obtain the formulae

$$\left.\begin{aligned} &-m\cdot\cos\vartheta\,\langle R_p^{m-1}(E,\cos\vartheta)\rangle \\ &= N\int d\sigma_{n,e}\int_0^{2\pi}\frac{d\alpha}{2\pi}\Big\{\langle R_p^m(E-T,\cos\vartheta\cos\varphi+\sin\vartheta\sin\varphi\cos\alpha)\rangle-\langle R_p^m(E,\cos\vartheta)\rangle\Big\}, \end{aligned}\right\} \quad (A.5)$$

$$\left.\begin{aligned} &-(m+1)\sin\vartheta\,\langle R_\perp^{m-1}(E,\cos\vartheta)\rangle \\ &= N\int d\sigma_{n,e}\int_0^{2\pi}\frac{d\alpha}{2\pi}\Big\{\langle R_\perp^m(E-T,\cos\vartheta\cos\varphi+\sin\vartheta\sin\varphi\cos\alpha)\rangle-\langle R_\perp^m(E,\cos\vartheta)\rangle\Big\}. \end{aligned}\right\} \quad (A.6)$$

The connection of the ranges $R_p(E,\cos\vartheta)$ and $R_\perp(E,\cos\vartheta)$ to the more interesting expressions $R_p(E)$ and $R_\perp(E)$, i.e. the ranges corresponding to initial angle $\vartheta = 0$, is given by Fig. 5.

$$\begin{aligned} R_p(E,\cos\vartheta) &= R_p(E)\cdot\cos\vartheta + R_\perp(E)\sin\vartheta\cdot\cos\beta, \\ R_\perp(E,\cos\vartheta) &= \Big\{\big[R_p(E)\sin\vartheta + R_\perp(E)\cos\vartheta\cos\beta\big]^2+\big[R_\perp(E)\sin\beta\big]^2\Big\}^{1/2}, \end{aligned}$$

where β is an azimuthal angle which is randomly distributed. We are interested in the case where the particle initially moves in the z-direction, i.e. we put $\vartheta = 0$ in (A. 5) and (A. 6):

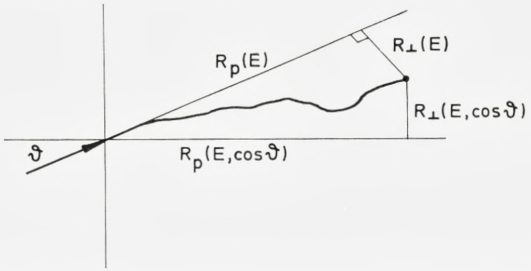

Figure 5. Illustration of connection between different range concepts.

$$m\,\langle R_p^{m-1}(E)\rangle = N\int d\sigma_{n,e}\left\{\langle R_p^m(E)\rangle - \langle R_p^m(E-T,\cos\varphi)\rangle\right\} \qquad (A.7)$$

$$0 = N\int d\sigma_{n,e}\left\{\langle R_\perp^m(E)\rangle - \langle R_\perp^m(E-T,\cos\varphi)\rangle\right\}. \qquad (A.8)$$

(A. 7) yields, for $m = 1$, the simple equation (4) for the average projected range, and $m = 2$ yields the two coupled equations

$$2\bar{R}_p(E) = N\int d\sigma_{n,e}\left\{\overline{R_p^2}(E) - \overline{R_p^2}(E-T)\cos^2\varphi - \tfrac{1}{2}\overline{R_\perp^2}(E-T)\sin^2\varphi\right\} \qquad (A.9)$$

$$0 = N\int d\sigma_{n,e}\left\{\overline{R_\perp^2}(E) - \overline{R_p^2}(E-T)\sin^2\varphi - \overline{R_\perp^2}(E-T)\cdot\frac{\cos^2\varphi+1}{2}\right\}. \qquad (A.10)$$

By introducing the ranges $\overline{R_c^2} = \overline{R_\perp^2} + \overline{R_p^2}$ and $\overline{R_r^2} = \overline{R_p^2} - \tfrac{1}{2}\overline{R_\perp^2}$, (A. 9) and (A. 10) finally read (cf. LSS)

$$2\bar{R}_p(E) = N\int d\sigma_{n,e}\left\{\overline{R_c^2}(E) - \overline{R_c^2}(E-T)\right\} \qquad (A.11)$$

$$2\bar{R}_p(E) = N\int d\sigma_{n,e}\left\{\overline{R_r^2}(E) - (1-\tfrac{3}{2}\sin^2\varphi)\overline{R_r^2}(E-T)\right\}, \qquad (A.12)$$

which equations may be solved separately if the source term $\bar{R}_p(E)$ is known, thereby giving $\overline{R_p^2}$ and $\overline{R_\perp^2}$.

References

N. Bohr, Mat. Fys. Medd. Dan. Vid. Selsk. **18**, no. 8 (1948).

Y. Y. Chu & L. Friedman, Nucl. Instr. Meth. **38**, 254 (1965).

B. Fastrup, P. Hvelplund & C. Sautter, to be published in Mat. Fys. Medd. Dan. Vid. Selsk. **35**, no. 10.

E. V. Kornelsen, F. Brown, J. A. Davies, B. Domeij & G. R. Piercy, Phys. Rev. **136**, A849 (1964).

J. Lindhard & M. Scharff, Phys. Rev. **124**, 128 (1961).

J. Lindhard, M. Scharff & H. E. Schiøtt, Mat. Fys. Medd. Dan. Vid. Selsk. **33**, no. 14 (1963).

J. Lindhard, Mat. Fys. Medd. Dan. Vid. Selsk. **34**, no. 14 (1965).

K. O. Nielsen, "Electromagnetically Enriched Isotopes and Mass Spectrometry", Butterworths, 1956.

J. H. Ormrod & H. E. Duckworth, Can. J. Phys. **41**, 1424 (1963).

W. R. Phillips & F. H. Read, Proc. Phys. Soc. **81**, 1 (1963).

Indleveret til Selskabet den 7. maj 1966.
Færdig fra trykkeriet den 28. oktober 1966.